Solar Physics (2005) 230: 91–109

THE TOTAL IRRADIANCE MONITOR (TIM): INSTRUMENT DESIGN

GREG KOPP and GEORGE LAWRENCE
Laboratory for Atmospheric and Space Physics, University of Colorado, Boulder, CO 80303
(e-mails: kopp@lasp.colorado.edu, lawrence@lasp.colorado.edu)

(Received 7 February 2005; accepted 13 May 2005)

Abstract. The Total Irradiance Monitor (TIM) instrument is designed to measure total solar irradiance with an absolute accuracy of 100 parts per million. Four electrical substitution radiometers behind precision apertures measure input radiant power while providing redundancy. Duty cycling the use of the radiometers tracks degradation of the nickel-phosphorous absorptive black radiometer interiors caused by solar exposure. Phase sensitive detection at the shutter frequency reduces noise and simplifies the estimate of the radiometer's equivalence ratio. An as-designed uncertainty budget estimates the instrument's accuracy goal. The TIM measurement equation defines the conversion from measured signal to solar irradiance.

1. Introduction

The total solar irradiance (TSI) is correlated with Earth climate and temperatures (Foukal, 2003; Lean, Beer, and Bradley, 1995). Proxies of the TSI based on sunspot observations, tree ring records, and cosmogenic isotopes provide estimates of the solar influence on the Earth that extend back thousands of years, and correlate with major climatic events on the Earth (Pang and Yau, 2002). Proxy TSI estimates upon which such correlations are based rely on accurate recent space-based solar irradiance measurements.

The Solar Radiation and Climate Experiment (SORCE) instrument suite, described by Woods *et al*. (2000), includes the Total Irradiance Monitor (TIM) to measure TSI with unprecedented precision and accuracy. This paper describes in detail the concept and design of the TIM instrument. Previous descriptions are given by Lawrence *et al*. (2000, 2003) and Kopp, Lawrence, and Rottman (2003). Calibrations with numerical results of the instrument's as-flown accuracy using on-orbit data are given in Kopp, Heuerman, and Lawrence (2005).

2. Design of the TIM

The TIM, shown in Figure 1, is an ambient temperature, electrical substitution, null-balance, solar radiometer. The instrument was designed to achieve 100 parts per million (ppm) combined standard uncertainty in TSI with a noise level of 1 ppm, largely achieved by good thermal design and the use of phase sensitive detection

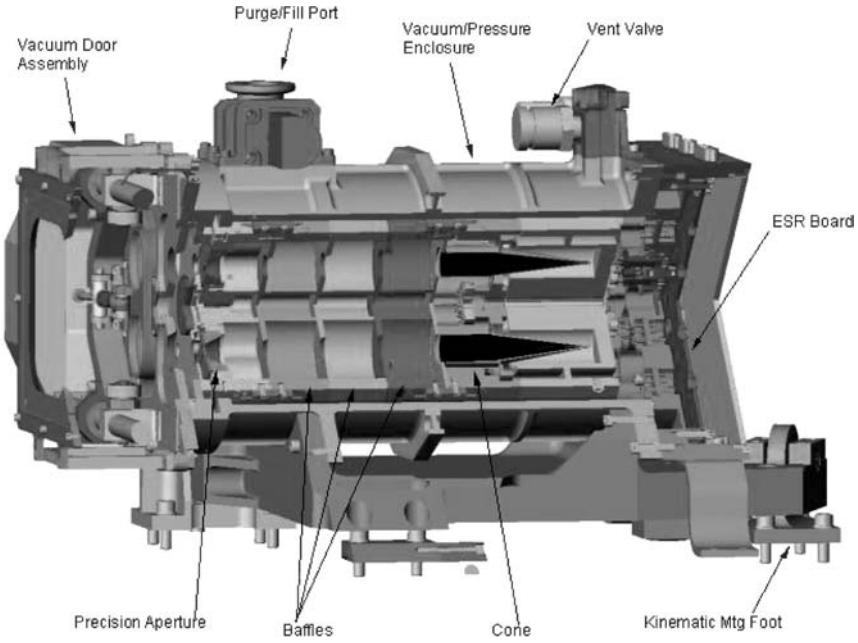

Figure 1. TIM cutaway. Four black absorptive cavities (two shown) measure solar power passing through precision apertures in a temperature-controlled instrument.

analysis techniques (Gundlach *et al.*, 1996). Four electrical substitution radiometers (ESRs) provide redundancy and allow degradation tracking via duty cycling. The ESRs are thermally balanced in pairs, one ESR of each pair acting as a thermal reference while the other is actively heated electrically to match this reference ESR's temperature. A 10-ms, bi-stable, open/close shutter operating with a 100-s period in front of a precision aperture in each ESR modulates sunlight entering that ESR's absorptive cavity. The reduction in electrical heater power needed to maintain the active ESR's temperature as its shutter opens and illuminates the ESR cavity interior with sunlight establishes the radiative power absorbed by the cavity; this electrical power decrease, combined with calibrations of the cavity's absorptance, is a measure of the entering radiant solar power. Phase sensitive analysis of the applied ESR electrical power at, and in-phase with, the shutter fundamental gives the incident radiant power while reducing sensitivity to noise and thermal drift. The precision aperture determines the area over which sunlight is collected. This area, combined with the measurement of incident radiant power, yields TSI in ground processing.

2.1. Absorptive cavities have high thermal conductivity

The TIM ESRs are thermally conductive cavities with high absorptivity across the entire solar spectrum. The high absorptivity ensures collection of nearly all the

entering sunlight, converting it into thermal energy in the cavity. The high thermal conductivity quickly transports this thermal energy to thermistors that monitor cavity temperature, so that the servo system maintaining the cavity temperature can respond quickly to changes. High thermal conductivity diamond at the thermal nodes also improves response. A wire-wound resistor embedded in the outer surface of each cavity's wall applies heat to the same region of the cavity as that heated by solar radiation. Matching the regions of the cavity electrically heated by the resistor with the region where sunlight is incident reduces the non-equivalence (the mis-match between radiant and electrical heat) and its uncertainty, and allows the thermal servo system to operate at higher gain by reducing overshoot.

The electrodeposited, 15.8 g ESR cavities are made mostly of silver, providing high thermal conductivity along the 6.34 cm axial cavity length. The rear conical section of each cavity is 4.06 cm long with a 10° half-angle, which helps trap the specular component of scattered light, increasing the cavity's absorptivity of entering light. A 2.29 cm cylindrical extension at the 1.6 cm diameter mouth reduces the sunlight scattering out of the cavity. The thermal conduction time from the sunlit rear of the cavity to the thermistors mounted near the cone/cylinder interface is about 2 s. A schematic representation of the cone geometry is shown in Figure A1.

The cavity interiors are etched nickel phosphorus (NiP), providing cavity reflectances of approximately 0.0002 averaged over solar wavelengths. Being a metal, NiP conducts absorbed radiant power into the body of the cavity quickly. Tests at the NIST Synchrotron Ultraviolet Radiation Facility indicate low degradation of this black absorptive layer to long-term exposure to sunlight. Reflectance calibrations of each cavity interior across the solar spectrum (Kopp, Heuerman, and Lawrence, 2005) correct for the sunlight not directly absorbed.

Stainless steel spoked mounts define the dominant thermal path to the TIM's heat sink, which is regulated to maintain a 31 °C set point temperature at the cavities. Temperature fluctuations of the heat sink at the shutter fundamental frequency are less than 10^{-6} K. Cavity thermal relaxation times through these mounts are measured to be approximately 220 s. All four cavities are cantilevered from a common central hub so that the active and reference cones have the same temperature source. Gold plating on the cavity exterior surfaces and on the instrument interior surfaces reduces radiative coupling between the cavities and their surroundings.

The four ESRs are separated by internal walls, so the light paths between the precision apertures and their corresponding cavities are isolated and independent. Three black baffles surrounding each ESR's light path block off-axis glint from the Earth or external instrument/spacecraft components. The baffle nearest each cavity contains a small silicon photodiode looking into the cavity to continually monitor that cavity's reflectance. The photodiode precision is $<0.1\%$ of the reflected light; so with a cavity reflectance of $\sim$0.0002 (200 ppm), the sensitivity to relative changes in absorptance is <0.2 ppm. These photodiode signals, corrected for their own degradation and in conjunction with simultaneous TSI measurements with pairs

of ESRs, monitor changes in cavity reflectances; results are described by Kopp, Heuerman, and Lawrence (2005).

2.2. MWS WIRE PROVIDES STANDARD RESISTANCE

Wound and encapsulated wire provides a resistive heater for each ESR cavity; applying a known voltage V across the heater leads heats the cavity with the power V^2/R, where each wire's resistance R is approximately 540 Ω. MWS Wire Industries 39-MWS-800-HML was selected for its measured $1.5 \times 10^{-5}\,^{\circ}\mathrm{C}^{-1}$ thermal coefficient of resistance, its stability over time, and its $<5 \times 10^{-6}$ hysteresis. A doubled strand of polyimide-insulated, resistive MWS wire is wound, under constant tension, in a tight spiral groove on the outside of each cavity's conical section, covering the area that is illuminated by sunlight in the cavity interior. This winding is epoxy encapsulated to maintain thermal conduction from the winding to the cavity. Over the heater windings, 200 nm of chrome and 0.013 cm of copper provide a base for the cavity's outer reflective gold plating, reducing radiative coupling to the cavity's surroundings.

Copper leads to the MWS heater wire contribute about 0.13 Ω (∼230 ppm) to the total circuit resistance. These are individually calibrated on the ground using four-wire ohmmeter connections. Four different instrument thermistors enable piece-wise corrections for copper resistance variations with temperature for calculating the effective flight resistance of these leads, yielding uncertainty in the lead resistance of <10 ppm.

2.3. LTZ1000 PROVIDES STANDARD VOLT

Two Linear Technology LTZ1000 voltage standards provide the reference voltage for each ESR pair. These thermostated, temperature regulated, buried Zener diodes supply 7.1 VDC with low thermal sensitivity and low drift. Spreadbury (1991) has shown their long-term stability to be better than 3×10^{-6} per year, and Rax, Lee, and Johnston (1997) have characterized their radiation stability. This high-precision voltage is digitally pulse-width modulated to the ESR heaters via a MOSFET switch having very low 0.004 Ω turn-on resistance, contributing a mere 7 ppm to the heater lead correction. The electrical heater power applied to an ESR from a reference voltage V is thus qV^2/R, where q is the digital signal processor controlled modulation duty cycle and can be varied between 0 and nearly unity.

2.4. PRECISION APERTURES DEFINE THE AREA OVER WHICH SUNLIGHT IS COLLECTED

Four diamond turned aluminum apertures of diameter 0.8 cm allow ≈ 68 mW of sunlight to enter each cavity. The flat sunward side of each knife-edge aperture is

highly reflective, reducing intrinsic heating. Each aperture is 0.76 cm thick, providing good thermal conductivity via an Indium gasket to the low-stress mounts to reduce thermal gradients. The 60° knife edge, with bevel facing the instrument interior, provides a precision area that is robust during machining and also prevents directly incident sunlight from reflecting off the specular interior aperture surfaces into the instrument. A resistive thermal device (RTD) mounted to the aperture mounting plate allows aperture area corrections due to temperature fluctuations after the apertures are characterized for their coefficient of thermal expansion. The 10.4 cm between the aperture and the cavity reduces both input stray radiation and corrections for shutter thermal emission, but comes at the expense of increased diffractive losses. Black baffles between the apertures and the cavities reduce stray light from off-axis objects such as the Earth.

2.5. SHUTTERS

Each ESR has an independent shutter, located immediately sun-ward of the precision aperture. These bi-stable shutters open or close in 10 ms. The thin aluminum shutters are low mass and mounted with low friction ball bearings. Accelerated life tests in thermal vacuum conditions exceed the SORCE mission lifetime of 5 years for cycles of the primary cavity's shutter by greater than a factor of 2. Gold plating on each shutter's interior surface reduces thermal emission into the instrument interior, while a thermistor embedded in each shutter allows correction for its thermal emission. Shutter open (10.0–11.0 ms) and close (9.8–10.8 ms) times are characterized and accounted for in the phase sensitive analysis.

2.6. DIGITAL CONTROL ELECTRONICS MAINTAIN THERMAL BALANCE

A 16 MHz Analog Devices TSC21020F–20MB/833 digital signal processor (DSP) performs all major instrument functions: thermally balancing the ESRs; regulating instrument temperature; maintaining shutter timing; and interfacing commands and telemetry with the spacecraft microprocessor. The DSP operates three 100 Hz AC servo bridges, which thermally balance the two paired ESRs and regulate instrument temperature. To maintain thermal balance, the DSP applies pulse-width modulated power to each cavity at 100 Hz via a field programmable gate array.

Since the solar irradiance is predictable to better than 1% during a given week, the estimated jump in replacement power is applied by the DSP at each shutter transition – a process called feedforward. This feedforward allows operation of the servo systems at high gain while preventing servo saturation during shutter transitions, and reduces sensitivity to uncertainty in the servo gain. By anticipating the decrease/increase in electrical power needed to maintain cavity temperature as a shutter opens/closes, the DSP's feedforward reduces the overshoot that would occur if the servo system only reacted to measured changes. The use of feedforward

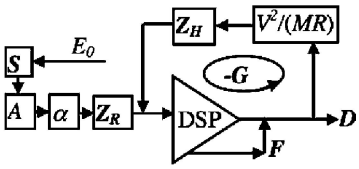

Figure 2. TIM signal transfer diagram. This signal transfer diagram illustrates the conversion from input solar irradiance E_0 to data numbers D. Variables in boxes are out/in ratios at some frequency. The servo loop gain is $-\boldsymbol{G}$. The digital signal processor (DSP) adds a known feedforward signal $\boldsymbol{F}$. The ratio of thermal impedances $\mathbf{Z_H}/\mathbf{Z_R}$ is the equivalence ratio. Bold symbols represent phasors.

essentially increases the effective servo loop gain and reduces the measurement uncertainty due to loop gain fluctuations. The instrument's signal transfer diagram including this DSP is shown in Figure 2.

To reduce the servo gain's sensitivity to operating temperature fluctuations, the thermistor bridge resistors are slightly asymmetrical so that the gain is at a maximum with respect to temperature at the nominal cavity operating temperature.

2.7. Phase-sensitive detection reduces noise

In ground processing, phase-sensitive detection of the electrical power applied to maintain ESR thermal balance gives the measured TSI. This method is similar to a Fourier analysis of a finite length of data. The TIM algorithm uses a filter that analyzes data in 400-s sections; this is long enough to benefit from some smoothing in the filter, much shorter than the time of an orbit, and comparable to time scales of short-term TSI variations, such as those due to solar oscillations.

The phase-sensitive detection method analyzes only changes in the applied ESR power at, and in phase with, the shutter fundamental frequency (0.01 Hz, or 100-s period). This method greatly reduces sensitivity to thermal drifts, $1/f$ noise, and parasitic thermal emission from the heat sink (which will be out-of-phase with the shutter). This detection method also means that the non-equivalence of heater and radiant power only needs to be known at the shutter frequency, making its calculation much simpler. Similar techniques are planned for the Scripps National Institute of Standards and Technology Absolute Radiometer (Scripps NISTAR) and have been used in an ambient temperature prototype (Rice, Lorentz, and Jung, 1999). The shutter frequency was selected near the minimum in the ESR-mounted thermistors' noise power spectrum, where noise levels reach a value of $\sim$1 ppm.

2.8. Equivalence need only be calculated at the shutter fundamental

The equivalence ratio, $Z_{\mathrm{H}}/Z_{\mathrm{R}}$, accounts for differences between electrical replacement heater power and absorbed radiant power. This ratio would be unity in an ideal

ESR; however, delays in thermal propagation for input electrical vs. radiant power can make this term differ significantly from unity, particularly at higher frequencies.

In the TIM ESR design, with the high diffusivity of the silver in the cavities and with both heater and radiant power inputs being nearly co-spatial at the cone end of the ESR, this ratio is within a few ppm of unity for signals in-phase with the shutter. The potentially large equivalence deviations at higher frequencies are not relevant, since one advantage of the phase sensitive detection method employed in the TIM analysis is that the instrument equivalence only needs to be known at the shutter frequency. This makes the calculation of the equivalence much easier and reduces uncertainties in this term.

Appendix A details the calculation of the TIM's equivalence ratio based on an algorithm developed in terms of known parameters of the ESRs.

2.9. TIM INSTRUMENT PERIPHERALS PROVIDE CORRECTIVE CAPABILITIES AND DIAGNOSTICS

The TIM ESRs, apertures, and shutters are the core of the instrument. Other items on the instrument help maintain thermal stability, maintain cleanliness, or give diagnostic information. A central heat sink maintains instrument temperature and stability both during a shutter's 100-s period and during the solar-illuminated and eclipsed portions of the 95-min SORCE orbit. A vacuum case with two vacuum doors maintains cleanliness of the instrument interior during integration and launch. Multi-layer aluminized mylar blanketing provides thermal isolation from the spacecraft's local environment. Multiple thermistors provide knowledge of various instrument temperatures, and are used in estimating thermal background corrections. Photodiodes monitor the cavity interiors for changes in reflectance, which might be indicative of a change in the absorptive NiP layer. A detector electronics board on the rear of the instrument contains the voltage references in close proximity to the ESRs to reduce the corrections for electrical leads supplying power to the cavity resistive heaters.

3. Relative Standard Uncertainties as Designed

Table I summarizes the combined standard uncertainty, σ, expected for the instrument as designed. Individual uncertainties are based on calibrations of prototypes, capabilities of state-of-the-art calibration facilities, analyses, and calculations using parameter uncertainties. (The actual uncertainties for the flight TIM are described by Kopp, Heuerman, and Lawrence (2005).) The dominant uncertainties are in the aperture area A and the cavity absorption α. The individual component uncertainties are assumed independent. Their quadrature sum gives a combined relative standard uncertainty of less than 100 ppm.

TABLE I

TIM uncertainty budget summary as designed (uncertainties are 1 standard deviation).

Factors/corrections	Size [ppm]	σ [ppm]
Distance (f_{AU})	33 537	0.1
Velocity (f_{Dopp})	57	0.7
Shutter waveform ($\boldsymbol{S}$)	100	1
Aperture (A)	1 000 000	55
Reflectance ($1 - \alpha$)	200	54
Servo gain ($\boldsymbol{G}$)	16 000	0
Standard (V^2)	1 000 000	7
Non-linearity	1 000 000	6
Standard R and leads	1 000 000	17
Equivalence ($\mathbf{Z_H}/\mathbf{Z_R}$)	7	22
Dark signal	1800	2
Scattered light	100	14
Repeatability (noise)		1
RSS total		84

4. TIM Measurement Equation

The TIM measurement equation follows from the signal transfer diagram shown in Figure 2. Scalars represent the input irradiance time series E_0, aperture area A, standard voltage V, standard resistance R, and a time series of output data numbers D. The bold-type terms are complex phasor components representing the amplitude and phase of sinusoidal variations as a function of frequency. These complex numbers describe shutter transmission $\boldsymbol{S}$, thermal impedances $\boldsymbol{Z}$, and servo gain $-\boldsymbol{G}$ within the instrument. TIM data and servo response are analyzed at frequencies between 10^{-4} and 50 Hz, but the irradiance is determined at the 0.01 Hz shutter fundamental. The data numbers D are output at rates up to 100 Hz, providing a maximum of 10^4 numbers per shutter cycle.

In ground data processing, the time series D is frequency analyzed and smoothed using a boxcar filter of the same period as the shutter, which eliminates sensitivity to changes at the shutter frequency. Four successive applications of this filter provide a nearly Gaussian weighting to the data within 200 s of a desired time (see Figure 3). Weighting by sinusoidal components at the shutter frequency produces the complex phasor $\boldsymbol{D}$ which provides knowledge of the changes occurring at, and in-phase with, the shutter fundamental. This data processing filter has the benefits of Fourier analysis at the shutter frequency while being able to analyze data within a 400-s interval.

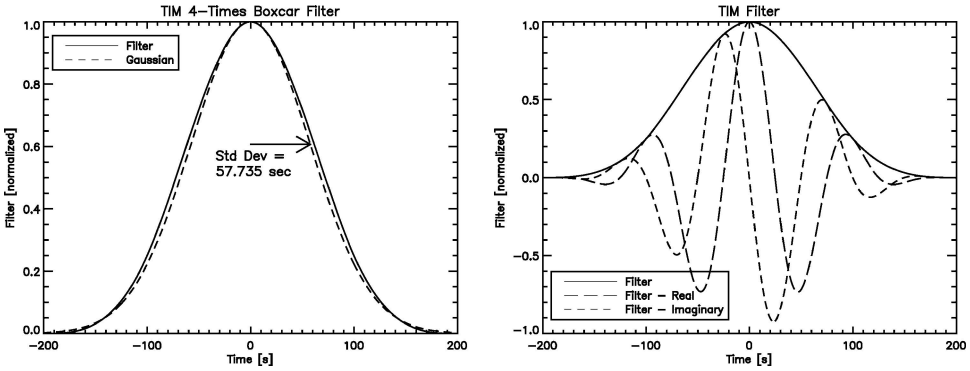

Figure 3. TIM data processing filter. This four-time repeated 100-s boxcar filter weights data with a near-Gaussian having total length of 400 s and a standard deviation of 57.7 s (*left plot*). Data in this range are Fourier analyzed to give changes at, and in-phase with, the TIM shutter fundamental (*right plot*).

The phasors $\boldsymbol{D}$ are converted to measured irradiances via

$$E_{\text{meas}} = \frac{V^2}{MR} \cdot \frac{1}{\alpha\, A f_{\text{corr}}} \cdot \text{real}\left[-\frac{\boldsymbol{Z_H}}{\boldsymbol{Z_R}} \cdot \frac{1}{\boldsymbol{S}} \cdot \left(\boldsymbol{D} + \frac{\boldsymbol{D} - \boldsymbol{F}}{\boldsymbol{G}} \right) \right], \tag{1}$$

which corrects for the complex servo system gain, shutter timing, equivalence $\boldsymbol{Z_H}/\boldsymbol{Z_R}$, applied feedforward values $\boldsymbol{F}$ at the shutter frequency, and scalar absorptance of the cavity α. Four correction factors are combined in f_{corr} to account for the spacecraft's distance to the Sun, Doppler shifts due to spacecraft velocity, cavity responsivity degradation, and pointing effects. The flight standard voltage V and the standard resistance R determine the standard watt, V^2/R. The fixed scalar $M = 64\,000$ converts data numbers D to duty cycle $q = D/M$; the standard voltage is applied to the active cavity's resistive heater at 100 Hz by a pulse width modulator.

Observations of empty space during the eclipse portion of each orbit provide a measurement of the instrument's thermal background. These thermal background measurements are modeled by four instrument temperature monitors. This empirical model, computed using instrument temperatures measured during actual solar measurements on the daytime side of the orbit, estimates the effective thermal signal appropriate for the solar observations, $E_{\text{dark\_est}}$. The reported TSI value is then the difference

$$E_0(t) = E_{\text{meas}}(t) - E_{\text{dark\_est}}(t). \tag{2}$$

5. Observation Modes and Data Products

The TIM's observation modes are summarized in Table II.

TABLE II
TIM observation mode summary.

Observation mode	Frequency	Duration	Target	ESR	Comments
Normal	Every orbit, daylight side	400 s per meas., continuous	Sun	B	Primary data acquisition mode
Dark	Every orbit, eclipse	400 s per meas., continuous	Dark space	B	Characterize thermal background
Degradation A	1%	1 orbit/week	Sun and dark space	A, B	Frequent degradation
Degradation C	0.5%	1 orbit/2 weeks	Sun and dark space	A, C	Infrequent degradation
Degradation D	0.2%	1 orbit/4 weeks	Sun and dark space	B, D	Infrequent degradation
Gain	Bi-weekly	4 orbits	NA	All	Servo calibration
FOV map	Every 6 months	15 orbits	Sun, 5×5 raster, $5'$ steps	B	Determine relative sensitivity to FOV

In SORCE's low Earth orbit of 640 km and 40° inclination, the TIM generally observes the Sun for the 'daytime' portion of every orbit; this is the 'Normal' mode. These sunlight periods last from 50 to 75 min of the orbit's 95-min duration. In this mode, the TIM uses its primary ESR, shuttered at the instrument's 100-s period, to acquire irradiance measurements of the Sun. A feedforward value appropriate for the expected solar irradiance level is used.

On the remaining portion of each orbit, during which the Sun is eclipsed by the Earth, the TIM acquires measurements of dark space using the same operational configuration as for the Sun but with a lower feedforward value. These measurements provide knowledge of the thermal, or 'dark,' contributions from the instrument that are used in correcting the measurements of the Sun.

At a 1% duty cycle, amounting to one orbit every week, the primary and secondary ESR are used simultaneously to measure TSI. This lesser-used secondary ESR has a lower rate of solar exposure, providing a stable monitor by which long-term variations in the primary ESR can be corrected. Similarly, the third and fourth ESRs are used at 0.5% and 0.2% duty cycles to monitor changes in the more frequently used ESRs. These modes are known as 'Degradation' modes. This degradation correction approach was first applied to TSI measurements by Willson (1979) and Willson *et al*. (1981) using the three cavities in the Active Cavity Radiometer Irradiance Monitor.

TIM servo gain is calibrated during a 6-hour period every 2 weeks (Kopp, Heuerman, and Lawrence, 2005). During this mode no solar observations are acquired. The instrument shutters remain closed, and each ESR's response to a square-wave electrical heater transition is measured. From this response, the servo gain is determined and monitored throughout the mission.

Every 6 months the SORCE spends several orbits performing a field of view (FOV) map to determine instrument sensitivity to pointing. This calibration is a 5×5 grid with 5-arc min spacings centered on the Sun. Measurements with each SORCE instrument at every grid position determine that instrument's pointing sensitivity and changes with time.

The TIM's primary data products are TSI in units of W m^{-2} reported at a constant distance of 1 AU from the Sun as well as the value measured at the top of the Earth's atmosphere. These are used for long-term studies of the Sun's output and for Earth climate modeling, respectively. Both daily and 6-hourly averages are reported. Reported uncertainties are based on the instrument's combined standard uncertainty and on the standard deviation of the Sun's output during the time period.

TSI values are computed at a 50-s cadence, from which the reported daily and 6-hourly values are computed by averaging valid data. Each measurement requires 400 s of data, or four complete shutter cycles, so these high-cadence values are not independent. The high cadence values are a research product and are useful for studying short-term solar features responsible for irradiance variations.

TIM TSI data are processed within a few days of acquisition and are available to the public after regular, frequent updates. Data are versioned such that any change

to the processing code or calibration parameters, such as when new degradation or gain data are applied, causes an increase in data version number. This configuration control links any data set with the associated parameters used in its generation.

The TIM data are available in ASCII text format online through the SORCE web site (*http://lasp.colorado.edu/sorce*) as well as through the NASA DAAC (*http://daac.gsfc.nasa.gov/upperatm/sorce/*).

6. Summary

The TIM design includes two significant improvements over previously flown TSI radiometers: (1) The use of phase sensitive detection lowers sensitivity to noise and thermal drifts and improves knowledge of the equivalence, and (2) NiP provides robust absorptive cavity interiors to withstand long-term exposure to solar radiation. This is the first space flight design intended to achieve 100 ppm combined standard uncertainty for an ambient temperature radiometer, and is made possible by exacting calibrations at the component level and extensive system design and analysis.

Appendix A: TIM Equivalence Calculation

In the TIM signal transfer diagram (Figure 2), measured signals from the combined heater power DV^2/MR and absorbed radiant power αE_0 are proportional to constants Z_H and Z_R, respectively. These (complex) thermal impedances Z are physical properties of the ESR and characterize its thermal response to input power. Both thermal impedances are frequency-dependent. The equivalence ratio, Z_H/Z_R, gives the conversion between replacement heater power and absorbed radiant power; this ratio would be unity in an ideal ESR. In the TIM ESR design, with the high diffusivity of the silver in the ESR and with both heater and radiant power inputs being nearly spatially co-located at the cone end of the ESR, this ratio is within a few ppm of unity for signals in-phase with the shutter.

The TIM's equivalence ratio, Z_H/Z_R, is calculated based on an algorithm developed in terms of known parameters of the ESRs. The computation proceeds by solving the thermal diffusion equation for power input at cavity position x, giving a Green's function solution, and then averaging the Green's function over the spatial distributions of input power. Thus, the three parts of the algorithm to calculate the equivalence ratio are the thermal Green's function $Z(x)$, and the normalized spatial distributions of electrical heat input $f_H(x)$ and radiant heat input $f_R(x)$. ESR parameters are varied over their uncertainty limits in a Monte Carlo program to calculate corresponding values of the equivalence ratio. The average of this ensemble is the final estimate of the equivalence ratio and the standard deviation of the ensemble is the uncertainty in the ratio.

Heat flow from the cone to the rest of the cavity can be treated as a one-dimensional (axial) problem because the four thermistors near the center of the ESR average out azimuthal temperature variations and because the initial power inputs are nearly azimuthally invariant. This approximation was verified numerically with two-dimensional finite element solutions and found to contribute less than 0.1% error to the calculated thermal impedances and hence has only a sub-ppm effect on the equivalence.

Another approximation is that heat from the replacement heater (embedded in the ESR's external surface) and heat from incident radiation (on the inside of the ESR) are taken to both have the same thermal impedance once the heat flows into the wall of the ESR. The relaxation time through this silver wall is on the order of 1 ms and the relaxation time through the inside NiP absorptive coating is only a few microseconds, which justifies this approximation for the TIM ESRs, having about 2-s net thermal response times.

The main difference in the two thermal impedances is from the heater wires, which are insulated from the silver wall in which they are embedded and have a thermal delay of about $\tau_{\text{wire}} \approx 20$ ms, as determined from finite element models. At the shutter fundamental of 0.01 Hz, this wire delay causes an amplitude attenuation of <1 ppm and a phase shift of 0.07°, creating about a 10 ppm shift in the equivalence ratio. Neglecting the microsecond NiP delay and the relaxation through the wall, the Green's functions for the heater wire and the radiative thermal impedances are then

$$Z_{\text{wire}} = Z(x)/(1 + i\omega\tau_{\text{wire}}), \tag{A.1}$$

and

$$Z_{\text{NiP}} = Z(x), \tag{A.2}$$

where $Z(x)$ describes the flow along the axial coordinate x in the wall of the ESR. Again, $Z(x)$ is the temperature signal at the thermistors divided by the power input at position x along the cavity. Because unit power is applied, $Z(x)$ is the desired thermal impedance between position x and the thermistors.

The use of sinusoidal signals (appropriate for the TIM's phase sensitive method) converts the diffusion equation from a partial differential equation in time and space to an ordinary differential equation in space. This is where the phase sensitive method of the TIM enables a much simpler estimate of the equivalence than allowed by more traditional, DC-subtraction based radiometers; with the phase sensitive detection method, the equivalence is only needed at one frequency, and the large equivalence variations at high frequencies are not relevant.

The heat flow (diffusion) equation for sinusoidal variations in the temperature of the cylinder portion of the cavity is

$$\frac{\mathrm{d}^2 Z}{\mathrm{d}x^2} = -\beta^2 Z, \tag{A.3}$$

where the complex wavenumber β (Equation (A.5)) characterizes both thermal conduction and thermal radiation from the outer surface of the ESR wall. The solutions of Equation (A.3) are the circular functions $\cos(\beta x)$ and $\sin(\beta x)$. Similarly, for the cone portion of the cavity the diffusion equation is

$$\frac{d^2Z}{dx^2} + \frac{1}{x}\frac{dZ}{dx} = -\beta^2 Z. \tag{A.4}$$

The basic solution of Equation (A.4) that is finite at the tip of the cone ($x = 0$) is the Bessel function $J_0(\beta x)$. For both the cone and cylinder portions of the cavity, β is defined by

$$\beta^2 = -\left(\frac{4\varepsilon\sigma T_0^3}{kW} + i\frac{2\pi f}{D}\right), \tag{A.5}$$

with D the effective thermal diffusivity of the cavity (mostly silver), f the frequency of interest, $4\varepsilon\sigma T_0^3$ the incremental surface radiant conductivity at operating temperature T_0, k the thermal conductivity of the ESR's silver, and W the wall thickness of the cone and cylinder portions of the ESR cavity. Thus, distributed radiation from the exterior surface is included in the formalism, assuming the emissivity is constant along the cavity. At the TIM shutter fundamental, $f = 0.01$ Hz, $\beta^2 \approx -(0.0001129 + i0.03696)\,\mathrm{cm}^{-2}$ and $\beta \approx (0.1357 - i0.1361)\,\mathrm{cm}^{-1}$.

The actual thermal impedance Green's function $Z(x)$ is constructed as linear combinations of the basic solutions by matching the boundary conditions at the junction of the cone and cylinder, including the conductivity Γ of the cavity support structure at this junction. Then, by averaging $Z(x)$ over the (normalized) distributions $f(x)$ of input power, the equivalence ratio is

$$\frac{Z_H}{Z_R} = \frac{1}{1 + i\omega\tau_{wire}} \frac{\int Z(x) f_H(x) dx}{\int Z(x) f_R(x) dx}. \tag{A.6}$$

Using the dimensions shown in Figure A1 and matching boundary conditions, relative solutions of the diffusion Equations (A.3) and (A.4) are, for inputs $x \le B$,

$$Z(x, x_T) = J_0(\beta x)\cos(\beta C - \beta x_T). \tag{A.7}$$

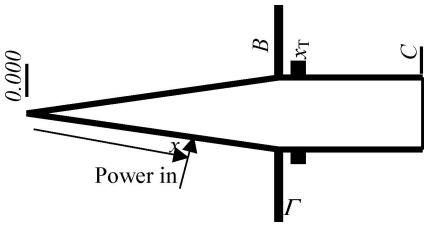

Figure A1. ESR cavity. With coordinate $x = 0$ at the apex of the cone portion of the ESR, the cone has slant length B, the ESR total length is C, and the thermistors are at x_T. The mechanical support, the heater leads, and the thermistor leads at B provide a thermal conduction of Γ to the surrounding instrument heat sink. Consider power input at some position x. The Green's function $Z(x, x_T)$ is then the temperature/power ratio between points x and x_T.

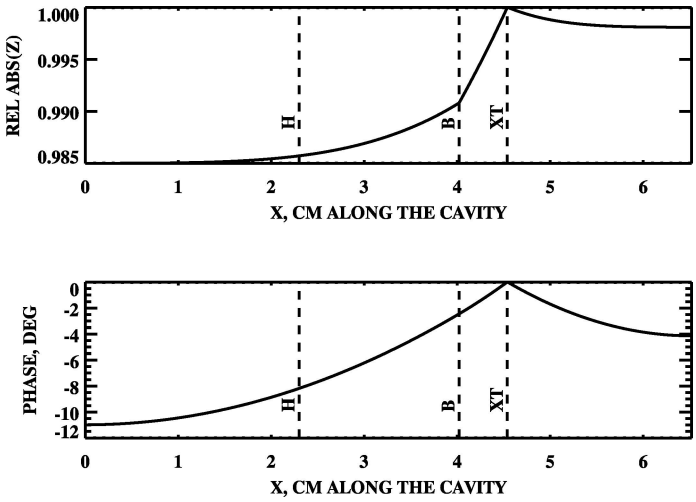

Figure A2. Thermal impedance. Relative thermal impedance to the thermistor as a function of input distance along the cavity for nominal parameters. B marks the cone/cylinder junction. XT is the location of the thermistors. H marks the nominal end of heat input.

For heat inputs on the cylinder ($x \geq B$), let x_{L} and x_{G} be the lesser and greater, respectively, of input position x and thermistor position x_{T}. For these positions x, the relative transfer impedance is given by

$$Z(x, x_{\mathrm{T}}) = \cos(\beta C - \beta\, x_{\mathrm{G}}) \times \\ \times\{\cos(\beta B - \beta\, x_{\mathrm{L}}) J_0(\beta B) + \sin(\beta B - \beta\, x_{\mathrm{L}})(J_1(\beta B) - \xi J_0(\beta B))\}, \tag{A.8}$$

where $\xi = \Gamma/2\pi\beta B k W \sin(\theta)$, with Γ the thermal conductivity of the cavity support located at $x = B$ and θ the half angle of the cone. The thermal impedance, $Z(x, x_{\mathrm{T}})$, of Equations (A.7) and (A.8) are plotted in magnitude and phase in Figure A2. The functions are even in the argument βx.

The heater distribution in x increases linearly along the axial coordinate x from x_1 to x_2, being from the wire wound resistor on the external portion of the cone and heating very nearly the same region around the apex as the incoming radiant power. The normalized heater distribution is

$$f_{\mathrm{H}}(x) = \frac{2x}{x_2^2 - x_1^2}, \quad x_1 \leq x \leq x_2. \tag{A.9}$$

In the actual TIM ESRs, there are about 1.5 turns of high pitch heater winding at the end nearest the cylinder to bring the wire (under the outer copper/gold plating) up to a low-resistance copper terminal strip and then to the heater lead connection at $x = B$. This extra heating is added numerically to the distribution and the entire distribution is normalized.

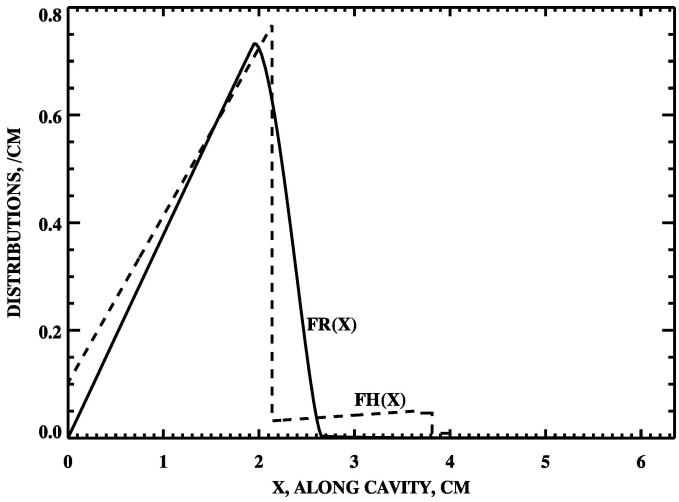

Figure A3. Heat distributions. Normalized distributions of heater power (FH) and absorbed radiant power (FR), given the nominal parameters of Table AI.

The incident radiant power distribution is nominally in a uniform cylindrical beam having a diameter defined by the precision aperture, but with fuzzy edges due to the finite size of the Sun. By design, this incoming solar beam has approximately the same uniform distribution as the electrical heater power, as shown in Figure A3. However, approximately 1.6% of the incident light scatters diffusely from the initial contact point, and this broadens the radiant heater distribution. For calculating equivalence, only the first bounce matters because the second bounce is reduced nearly another 2 orders of magnitude. For a total hemispherical Lambertian reflectance η at the first bounce, the distribution becomes

$$f_{\text{RAD\_DIFFUSE}}(x) = (1-\eta)\frac{2x}{H^2} + \eta\, f_{\text{DIF}}(x), \tag{A.10}$$

where H is the length of the illuminated area measured axially. $f_{\text{DIF}}(x)$ is the first bounce scatter distribution derived from the Lambertian scattering and the conical geometry, and is given by

$$f_{\text{DIF}}(x < H) = \\ = -\frac{H^2 - (H-2x)(x+Y) + H(H-3x-Y)\cos(2\theta) - 4xY\sin(\theta)}{2\tan(\theta)H^2Y} \tag{A.11}$$

and

$$f_{\text{DIF}}(x > H) = \\ = \frac{H^2 - Hx + 2x(x-Y) + 2HY\cos^2(\theta) + H(H-3x)\cos(2\theta)}{2\tan(\theta)H^2Y}. \tag{A.12}$$

TABLE A1

Parameters and their uncertainties for equivalence calculations (all uncertainty distributions are assumed uniform and rectangular to the ±limits, and all are assumed independent.).

		Nominal	Distribute	
Equivalence Model Parameters				
K	Thermal conduction, silver	4.27	±10%	$W\,c^{-1}\,K^{-1}$
B	Slant distance, cone vertex to cylinder	4.06	±0.2	cm
XT	Slant distance, vertex to thermistor	4.54	±0.2	cm
C	Slant distance, vertex to cone mouth	6.35	±0.2	cm
D	Diffusivity of silver + copper plate	1.6	±10%	$cm^2\,s^{-1}$
EPS	IR emissivity of the cone exterior	0.04	±0.02	
W	Wall thickness	0.07	±0.02	cm
Tau	Zero-order pole time constant	220	±10%	s
C_H	Specific heat of the cone/cylinder	0.26	±10%	$J\,g^{-1}\,K^{-1}$
	Mass of the cone assembly	15.78	±10%	g
H	Slant distance to edge of light beam	2.3	±0.1	cm
Tau_wire	Time constant of heater wire	20	±10	ms
Heater Winding Geometry				cm
	Uncertainty in the vertex position		±0.1	cm
S0	Start of cone winding	0.329	±0.01	cm
R0	Radius of winding at the start	0.058	±0.01	cm
S1	End of fine pitch winding, start fast pitch	2.465	±0.01	cm
R1	Radius of fine pitch winding at the end	0.435	±0.01	cm
S2	End fast pitch, start leads	4.012	±0.01	cm
R2	Radius at end of fast pitch	0.73	±0.01	cm
S3	Copper strap start	4.141	±0.01	cm
S4	Copper strap end	4.217	±0.01	cm
S5	Heater lead terminal point	4.349	±0.01	cm
η	NiP black total hemispherical reflectance	0.02	±0.01	

θ is the cone half angle and the auxiliary length Y is defined as

$$Y = \sqrt{H^2 + x^2 - 2Hx\cos(2\theta)}. \tag{A.13}$$

The total integral over dx of this formula is slightly less than one because of some escape out the front of the cone. This escaped fraction is accounted for separately by the calibration cone absorptance factor α. Because of this, numerical calculations must renormalize the distribution's area to one.

Based on this formalism, the total reflected loss out the front will be $1 - \alpha \approx 1.23\%$ of η, a result consistent with non-sequential ray trace studies. For example, a Lambertian reflectance $\eta = 1.6\%$, consistent with bidirectional reflectance

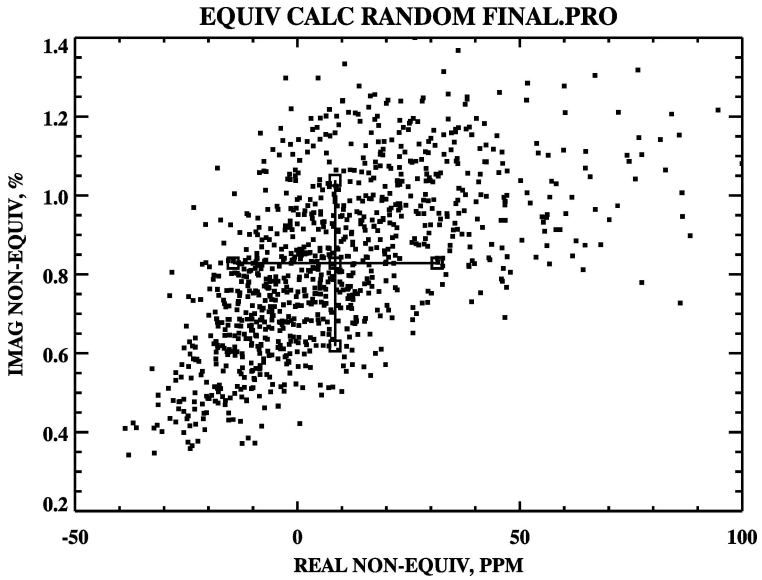

Figure A4. Equivalence estimate. Monte Carlo calculation of the "non-equivalence", $Z_H/Z_R - 1$. The cross in the center indicates the average and ± 1 standard deviation of the ensemble.

distribution function measurements of NiP, would give a total ESR reflection loss $1 - \alpha = 250$ ppm, close to the calibrated values for the TIM ESRs.

There should also be a thermal IR radiation term included in the definition of β to account for IR losses out the mouth of the ESR. In the analytic solution (A.5), β characterizes the constant emissivity of the gold-plated exterior of the cone, but neglects the effect of thermal radiative emission of the cone from the interior surface. The total radiative conduction in the front is

$$\Gamma_{\text{IR\_mouth}} < \pi\, R^2_{\text{mouth}} \times 4\sigma\, T_0^3 \approx 0.0011\,\text{W K}^{-1}. \tag{A.14}$$

The measured total conductivity of the cone support is $\Gamma_{\text{total}} \approx 0.016\,\text{W K}^{-1}$, so the interior IR conductivity is approximately 7% of the total. This radiative conduction is distributed proportional to the view factor from the interior to the outside. Analysis shows it to come mostly from the centimeter of the cylinder nearest the mouth of the cavity. This is removed as far as possible from the heat distribution functions within the cone, so does not provide a significant effect on the equivalence ratio.

Inclusion of this distributed IR gives the diffusion equation a wavenumber β that varies slightly with x, requiring a numerical rather than an analytic solution. Numerical solutions obtained using finite element methods and sparse matrices ($18\,000 \times 18\,000$) verified the analytic model and showed that the addition of the IR distributed conductivity changes the equivalence ratio by less than 1 ppm. The distributed IR radiation is therefore neglected in the determination of Z_H/Z_R.

Additionally, in the Monte Carlo calculations, the support conduction Γ is assigned an uncertainty of $\pm 10\%$, which accommodates the distributed 7% IR loss near the mouth of the cavity.

The analytic result enables a Monte Carlo uncertainty analysis of the equivalence ratio. The parameterized thermal impedance given by Equations (A.7) and (A.8), and the distribution of heater power (Equation (A.9)) and of absorbed radiation (Equations (A.11) and (A.12)) yields an equivalence ratio given the set of parameters and their uncertainties listed in Table AI.

From the distributions of parameters listed in Table AI, an ensemble of 1000 equivalence ratios was computed at the shutter fundamental, giving the average and standard deviations shown in Figure A4. This gives an equivalence ratio for the TIM of

$$Z_{\mathrm{H}}/Z_{\mathrm{R}} = (1.000008 \pm 0.000023) + i(0.0083 \pm 0.0021). \tag{A.15}$$

Acknowledgements

This research was supported by NASA contract NAS5-97045. Informal reviewers from NIST and NASA provided much useful advice. LASP engineers are greatly acknowledged for their major contributions to the instrument design and function.

References

Foukal, P.: 2003, *EOS Trans. AGU* **84**, 22, 205.
Gundlach, J. H., Adelberger, E. G., Heckel, B. R., Swanson, and H. E.: 1996, *Phys. Rev. D*, **54**, R1256.
Kopp, G., Heuerman, K., and Lawrence, G.: 2005, *Solar Phys.*, this volume.
Kopp, G., Lawrence, G., and Rottman, G.: 2003, *SPIE Proc.* **5171**, 14.
Lawrence, G. M., Rottman, G., Harder, J., and Wood, T.: 2000, *Metrologia* **37**, 407.
Lawrence, G. M., Kopp, G., Rottman, G., Harder, J., Woods, T., and Loui, H.: 2003, *Metrologia* **40**, S78.
Lean, J., Beer, J., and Bradley, R.: 1995, *Geophys. Res. Lett.* **22**, 3195.
Pang, K. D. and Yau, K. K.: 2002, *EOS Trans. AGU* **83**, 43, 489.
Rax, B. G., Lee, C. I., and Johnston, A. H.: 1997, *IEEE Trans. Nuclear Sci.* **44**, 1939.
Rice, J. P., Lorentz, S. R., and Jung, T. M.: 1999, in: 10th Conference on Atmospheric Radiation, 28 June–2 July, Madison, Wisconsin (Preprint volume).
Spreadbury, P. J.: 1991, *IEEE Trans. Instrum. Meas.* **40**, 343.
Willson, R. C.: 1979, *J. Appl. Opt.* **18**, 179.
Willson, R. C., Gulkis, S., Janssen, M., Hudson, H. S., and Chapman, G. A.: 1981, *Science* **211**, 700.
Woods, T., Rottman, G., Harder, G., Lawrence, G., McClintock, B., Kopp, G. *et al.*: 2000, *SPIE Proc.* **4135**, 192.